Concurrent Flame Spread Over Two-Sided Thick PMMA Slabs in Microgravity

Concurrent flame spread over two-sided thick PMMA slabs in microgravity

Sandra L. Olson*, David L. Urban, Gary A. Ruff
NASA Glenn Research Center, Cleveland, OH 44135, USA
and
Paul V. Ferkul
USRA, NASA Glenn Research Center, Cleveland, OH 44135, USA
and
Balazs Toth
European Space Agency, Noordwijk, Netherlands, Postbus 299, NL-2200 AG.
and
Christian Eigenbrod, Florian Meyer
ZARM - University of Bremen, Bremen, Germany, Am Fallturm, D-28359 Bremen.
and
Grunde Jomaas
School of Engineering, University of Edinburgh, Edinburgh, EH9 3FG, UK.

*Corresponding Author: Sandra L. Olson,
Sandra.olson@nasa.gov
Fax (216) 433-8060
Phone (216) 433-2859

Concurrent flame spread over two-sided thick PMMA slabs in microgravity

Spacecraft fire safety is an important consideration when designing future exploration spacecraft. Concurrent flow flame spread experiments were carried out aboard the Cygnus spacecraft while in orbit to address current knowledge gaps related to solid fuel combustion in microgravity. The experiments used PMMA (polymethylmethacrylate) samples that were 50 mm wide and 290 mm long with two variations – one sample was a 10 mm thick flat slab, while the other was a 10 mm thick flat sample that had a 4 mm thick grooved center section. The thickness variation had a major impact on the flame shape, and the grooved sample developed a deep inverted-V shaped notch as the thin center section burned through. This notch enhanced heat transfer from the flame to the solid through an effectively wider flame base, which is the part of the flame with the highest temperature. Unlike in normal gravity (and also likely in partial gravity), where buoyant flow promotes acceleratory upward flame growth, the microgravity flames reached a steady size (limiting length) for a fixed forced convective flow in agreement with theory (i.e. there is a zero net heat flux at the flame tip). The limiting length implies that the spread rate of the flame will be controlled by the regression rate (burnout rate) of the material because the flames remains anchored to the upstream end of the fuel samples. This is a significant finding for spacecraft fire safety, and makes the probability of flashover in a spacecraft unlikely as the flame size will be small for low convective ventilation flow environments typical in spacecraft. On the other hand, long-burning flames in small vehicles will generate significant quantities of fuel vapor that may reach the lean flammability limit and cause a backdraft. The rapid extinction of the flame when the flow was turned off also supports the existing fire mitigation strategy on the ISS to deactivate the ventilation system in the event of fire alarm. These findings can be applied to improve the safety of future space exploration missions.

Keywords: concurrent flame spread, microgravity, PMMA, thermally thick

1. Introduction

IT is not possible to eliminate all flammable materials from use in spacecraft, so storage of flammable materials on the International Space Station (ISS) is carefully controlled, and potential ignition sources are rigorously screened for safety [1]. NASA STD-6001 Test 1, similar to other international standard tests [2-4], is a normal gravity upward flame spread test that uses a 50 mm x 300 mm long flat sample to evaluate a material's flammability in the spacecraft atmosphere (pressure and oxygen concentration). However, the normal gravity test has an inherent buoyant flow that is not present in orbiting spacecraft. NASA has been working to understand the importance of spacecraft ventilation, an integral part of the spacecraft's life support system, on a material's flammability, so one of the primary variables of the Saffire flight experiment [5] described in the current study is the forced flow past the large scale samples.

Microgravity flame spread over thick fuels has historically been limited to small samples (< ~ 100 mm long) and has most often been studied in opposed flow geometries [6-9]. Thermally-thick fuels, defined as having a non-uniform internal temperature distribution, have a characteristic dimension greater than 3 mm, such as a half-thickness for two-sided burning (not that the samples used are not infinitely-thick). These thick fuels typically require long experimental durations for flame spread studies in low gravity due to the long solid phase thermal response time. The available microgravity concurrent thick fuel tests are in a cylindrical geometry [10-13], but most practical flight materials are flat surfaces rather than cylinders.

Markstein and de Ris [14] showed for a very large thermally thin fuel that a steady flame size can be reached for normal gravity upward (concurrent) flame spread. Saffire flights I-III [15] demonstrated that a steady flame size can also be obtained in microgravity for a thin fuel in concurrent flow. However, in normal gravity, upward flame growth over thermally thick fuels is generally acceleratory and turbulent except for the first 100 mm or so of the spread [14-

16]. An exception is the horizontal concurrent flow tests with a thick fuel which found steady flame spread [17, 18] since the orthogonal buoyant flow does not contribute to the convective heating of the downstream fuel.

Numerical models have shown that quiescent microgravity flame spread over thick fuel slabs is unsteady [6]. However, experimental flames burning thick fuels become steady for even low flow velocities (10 mm/s) [8-10]. Thick fuel concurrent flame spread has been modeled [19-22]. Flame spread over simulated thick fuels was also modelled using the classic Emmons problem geometry [23].

The current study presents results from two experiments conducted as part of Saffire II (see Section 2) in order to investigate concurrent flame spread over two thermally thick, large PMMA slabs in a 101 kPa air flow of 200 mm/s, which is typical of the ISS environment with the ventilation on [24]. Of particular interest is how large the flame will grow over the thick fuel, and whether it will reach a steady flame size, as was predicted for forced convective concurrent flow [21, 22]. The questionable premise that a flat sample is representative of the worst case geometry, as opposed to samples with exposed edges/corners, was also studied.

PMMA was selected for these thick fuel tests because it is a classic non-charring fuel, and it is also currently the leading candidate for future spacecraft interior windows due to its low mass, strength, and optical properties. One of the two samples was a flat sample, and the second sample was a grooved sample, with exposed edges and interior corners and varied fuel thickness.

A number of normal gravity upward flame spread tests were performed on identically shaped and held samples of both kinds [25-27]. Eigenbrod and co-workers [25, 26] found that the normal gravity samples were only allowed to regress less than 10 mm, but during that time the pyrolysis front spread over 180 mm (measured with an infrared camera tracking the 330°C surface temperature). In addition, preferential edge/corner pyrolysis front spreading was noted on the exposed edges, and the fastest spread was along the interior groove edges rather than the centerline. The flame length was increasing rapidly in time for the 1g tests [25]. The reported 1g data did not reach a steady state flame size. The normal gravity pyrolysis front propagation velocity along the centerline of the grooved samples was 70% higher than that of the flat sample as the flame spread preferentially along the exposed edges. The 1g burnout velocities (base spread rates) [25] were 0.03 mm/s for the thick part of the grooved sample as well as the flat sample, and the centerline 4 mm thick section developed a notch due to a higher burnout velocity of 0.08 mm/s. Thomsen et al. [27] varied the pressure, and the comparable 100 kPa tests also had continued flame growth over the sample so that the flame did not reach a steady size. Through scaling arguments, the mixed convective flow for the 100 kPa test was estimated to be 820 mm/s, much higher than the 200 mm/s tested in Saffire II.

Upward flame spread over a thermally thick sample primarily spreads over the surface in 1g as there is always enough air entrainment through turbulence for an increasing flame length and increasing material consumption. In microgravity, this buoyant air entrainment does not occur, and the mechanisms of flame spreading may be quite different. The goal of these tests is to improve fire safety in human spaceflight by better understanding the mechanisms of flame spread over thick fuels.

2. Experiment Description

Saffire II was the second in a series of flight experiments being conducted by NASA to study flame spread under microgravity conditions. The Saffire II flight experiment was launched aboard Orbital ATK's OA5 'S.S. Alan G. Poindexter' on October 17, 2016. After spending a month docked to the ISS, it departed the ISS on Nov. 21, 2016, and Saffire II was successfully conducted once the vehicle had clear orbits outside the South Atlantic Anomaly. The experiment ran autonomously with a prescribed sequence. After the samples were tested, the digital data and some of the image data were downlinked over the next few days as the vehicle passed over ground stations set up to receive the data. Not all of the image data could be downloaded because of the limited capability in the given timeframe for downlinking.

The Saffire flow duct schematic is shown in Fig. 1. The sample card was in the center of the flow duct, and the location of the PMMA samples is shown in gray. The flow was from right to left, drawn through the duct by

downstream fans. Other near-field diagnostics used for these tests included a color camera (0.44 mm/pixel for each sample), radiometers, and thermocouples. The camera and radiometers (front and back) captured the data from the PMMA tests. A blinking green LED strip illuminated the front of the samples so that some dark frames and some lit frames of the tests were captured.

The orthogonal schematic of the sample holder, which held 9 samples, is shown in Fig. 2. It was made of two 0.8 mm thick aluminum sheets which were painted flat black on the exposed surfaces. Samples 1-4 were silicone samples of different thicknesses, samples 5 and 6 were a SIBAL cloth (a cotton fiberglass blend), sample 7 was a staged sample with a thin PMMA ignition strip and a Nomex HT90-40 downstream section. The preliminary results of all 9 tests have been reported [28], while the current study is focused on the final results for samples 8 (grooved) and 9 (flat). The radiometers' approximate field of view is outlined in red. Thermocouples on samples 5 and 6 are shown, since they are used herein. They were type R, 5 mm bare wire, woven into the surface, with the leads perpendicular to flame

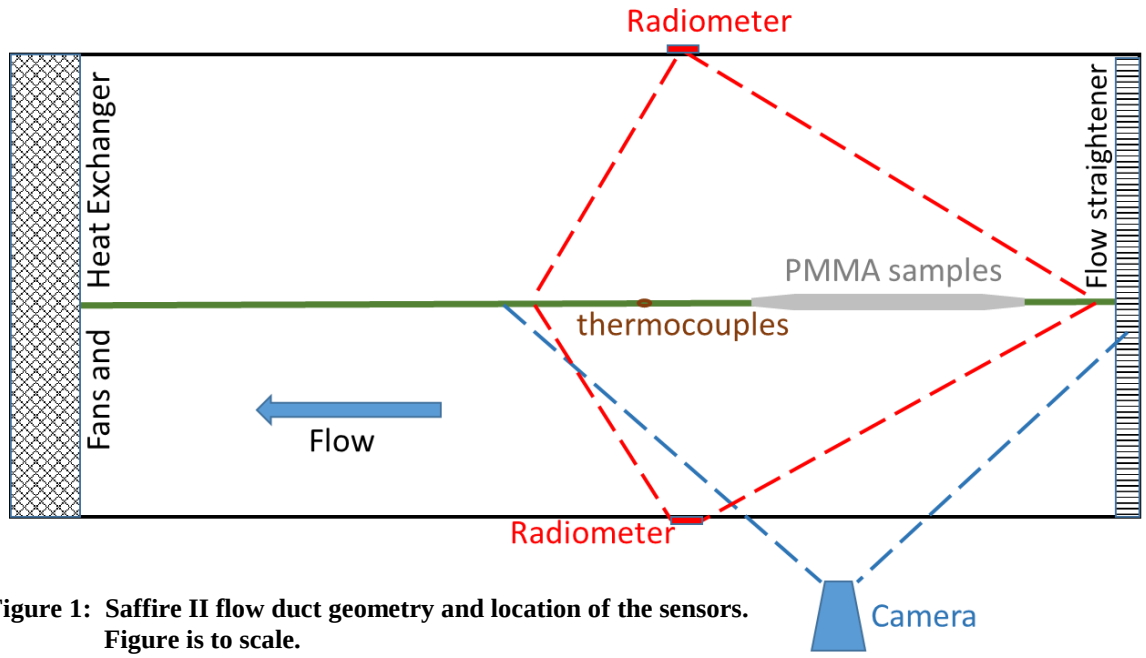

Figure 1: Saffire II flow duct geometry and location of the sensors. Figure is to scale.

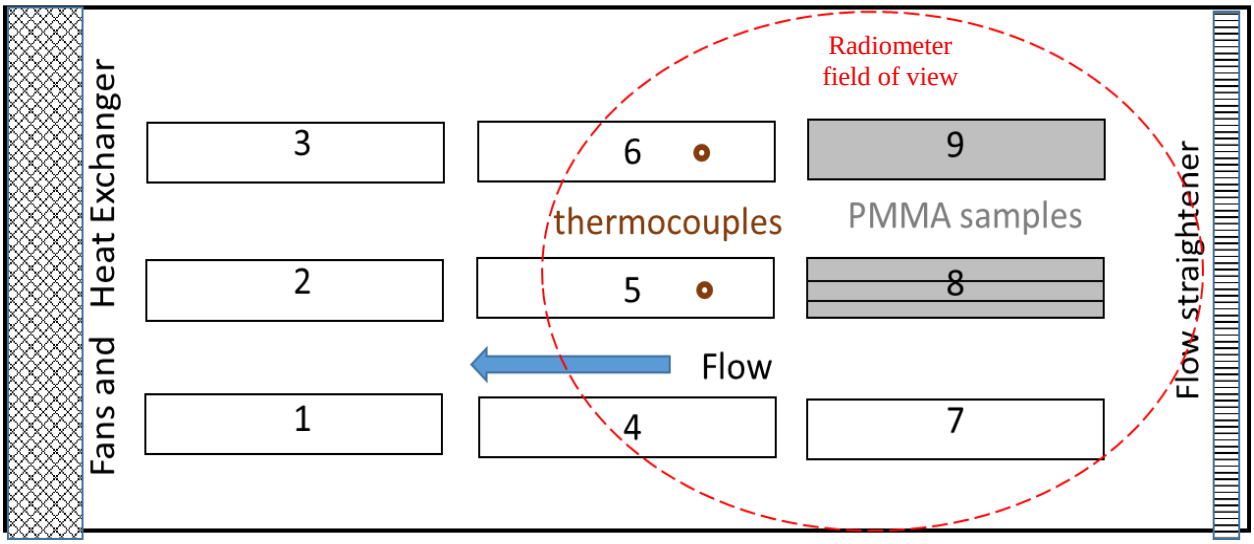

Figure 2: Sample card showing location of the two PMMA samples (in gray). Figure to scale.

spread direction to minimize conductive losses down the leads. The flow was again from right to left. Upstream of each igniter was a 10 mm ± 1 mm air gap in the holder to minimize ignition end heat losses.

Both clear cast PMMA samples were 50 mm wide and 290 mm long. As shown in Fig. 3, the ends were tapered so that the air could flow smoothly over the samples, which are thicker than the sample card. The upstream ignition end (~ 9 mm total length) was tapered to a 4 mm x 4 mm edge through which the igniter was threaded. The 29 gauge Kanthal A-1 igniter was activated for 30 seconds at 3.67 amps for each sample. Sample 9 was a plain flat slab, and sample 8 was a grooved PMMA sample with thickness variation and radius of curvature variation, as shown in Fig. 3. Both samples were mounted to a C-shaped 8 mm aluminum bracket that was sandwiched between the sample holder sheets. The grooved sample had exposed edges of different radius of curvature like the normal gravity comparison tests. For the flat PMMA sample, the side edges were inhibited by a 0.8 mm thick aluminum sheet. The edge pieces had slots cut in so that a C-shaped bracket with tabs could be inserted into the slots to support the sample.

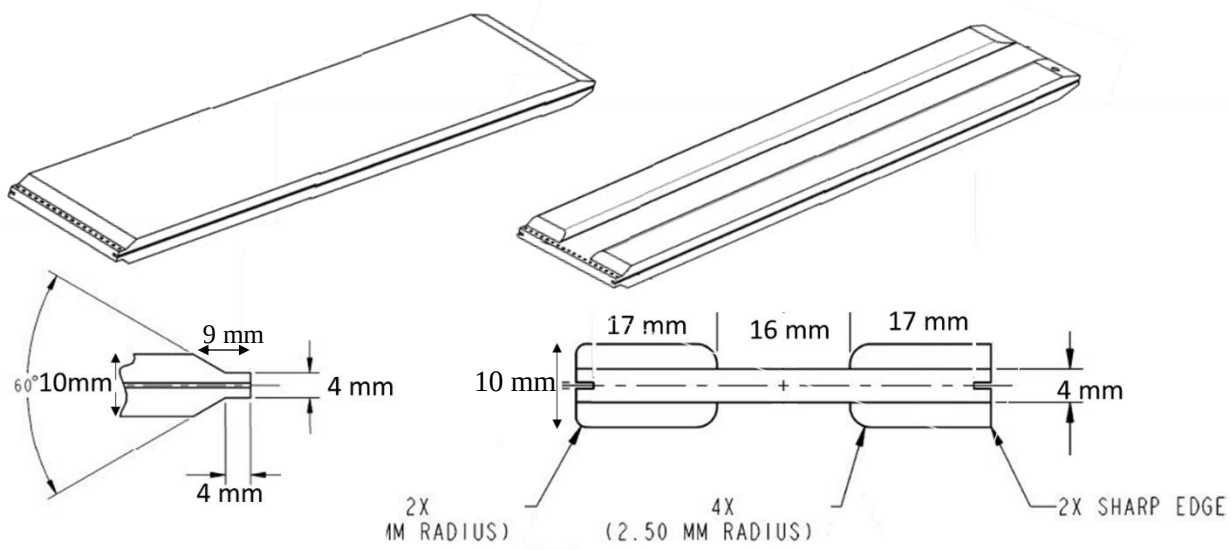

Figure 1: Details of the lain flat slab sample 9 (left) and grooved sample 8 (right). The lower left schematics show the ignition end detail, and the lower right schematic shows the cross section of the grooved sample 8.

Samples 8 and 9 were the last two samples burned in the pre-programed sequence of Saffire II. The experiment with the grooved sample 8 lasted 600 s (10 min), while the experiment with the flat sample 9 was allowed to run for 900 s (15 min). At hatch closure prior to undocking, the atmosphere was 22.1% O_2, 100.6 kPa, and RH 43% at 22.6 ºC.

The forced flow velocity for each test was set to 200 mm/s. However, from the anemometer readings shown in Fig. 4a, the flow on the two sides of the grooved sample appears to slowly diverge after ignition, and continued to diverge throughout the test by up to ± 15 mm/s. The flow was turned off to extinguish the flame to end the test. The flow remained off for approximately 60 seconds before it was turned on at the beginning of the experimental sequence for the flat sample 9. Notice that the anemometers continued to read a decaying offset until well into the experiment with the flat sample. Approximately 400 s into the test, as shown in Fig. 4b, the flow on the two sides of the duct was approximately equal for the remainder of the test. Potential causes of this divergence will be discussed later.

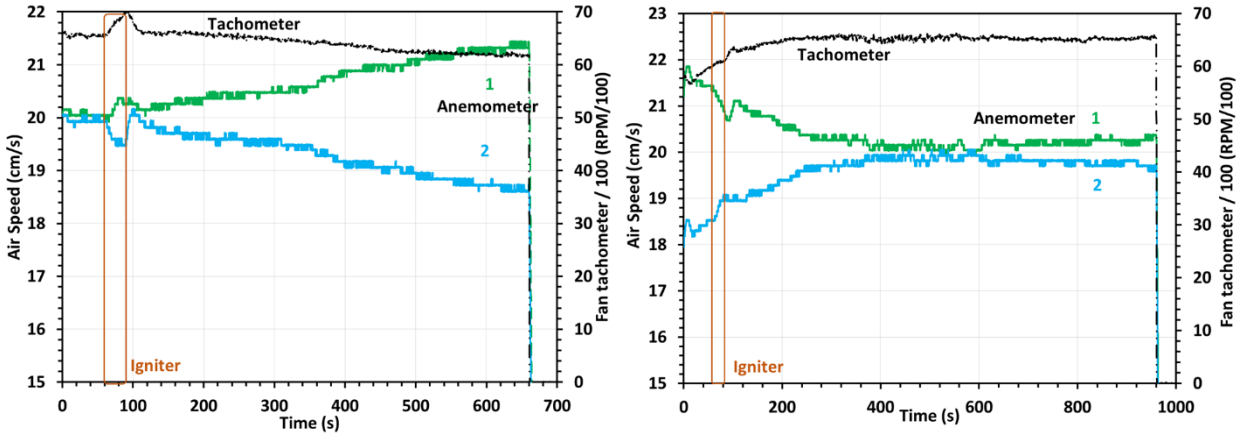

Figure 2: Flow readings for a) grooved sample 8 (left) and b) flat sample 9 (right) relative to ignition for each sample. Anemometer 1 is on the 'back', while anemometer 2 is on the 'front' camera side.

3. Flame appearance and tracking

All still frames were mapped to a scale to correct for the fisheye lens distortion. Two cameras were used to image all nine samples, and the image resolution was 0.447 mm/pixel. The flat sample (9) had more distortion to correct than the grooved sample (8) due to its position on the sample card. Dark images were intended to show the flame, and lit images were intended to show the degrading PMMA surface. However, the flames were quite luminous at the 200 mm/s air flow, so the camera exposure was controlled by the sooting of the flame and not the LED lighting, and more so for the grooved sample 8 than the flat sample 9. The exposure times for the grooved sample were 5 ms ± 2 ms after the apparent steady flame length at 300s, whereas exposure times for the flat sample were 15 ms ± 2 ms from 600-800s, and decreased to 11 ms ± 2 ms after 800s as the igniter coil glow began to fade as the flame base began to move away from the igniter wire. Both sample images had zero gain. These exposure times indicate that the flame was brighter for the grooved sample than for the flat sample.

3.1 Flame Images

The processed flame images are shown in Fig. 5. The leftmost four images are from the grooved sample 8 (unburned lit, burned lit, late flame unlit and late flame lit), and the rightmost four images are from the flat sample 9, in reverse order (late flame lit, late flame unlit, burned lit and unburned lit). The burned lit images show an almost triangular burnout region for the grooved sample and a flat burnout region for the flat sample. The distance from burnout to the clearly visible centerline bubble at the end of the pyrolysis region for the grooved sample was 78 mm and 76 mm for the flat sample. Both samples had significant soot deposits tapering along the length of the material and extending onto the downstream already-burned SIBAL samples.

The maximum burnout distance for the grooved sample 8 was 30 mm ± 1 mm downstream of the initial upstream sample end, while the side burnout distance was 15 mm ± 1 mm. Both of these are beyond the 9 mm igniter end region (4 mm ignition tongue plus 5 mm long tapered section, see Fig. 3). The burnout for the flat sample 9 was 12 mm ± 1 mm downstream of the initial upstream sample edge, only a few mm past the tapered region. The flame standoff distances, estimated from the last images of the upstream edge of the bright luminous flame base to the post-extinction burnout PMMA edge, were 8 mm ± 1 mm for both the centerline of the grooved and the flat sample, tapering to 5 mm ± 1 mm near the edges of the grooved sample. These estimates do not include any outer blue flame that may be present but are not captured by the camera.

The images show that the grooved sample had a parabolic shaped flame tip and a notched burnout region where the thin center section burned through much further downstream than the thicker sides. The flat sample had a similar parabolic flame tip and a flat base. The lit image for the grooved sample has a darker green background illumination

due to the more luminous flame controlling the camera exposure. The very dim tip of the flame is slightly easier to see in the dark images than the lit images from the same time. It is important to point out that the flame remained anchored to the upstream end of the fuel sample throughout the test. As will be shown later, this anchoring limits the spread rate of the flame to the base regression rate.

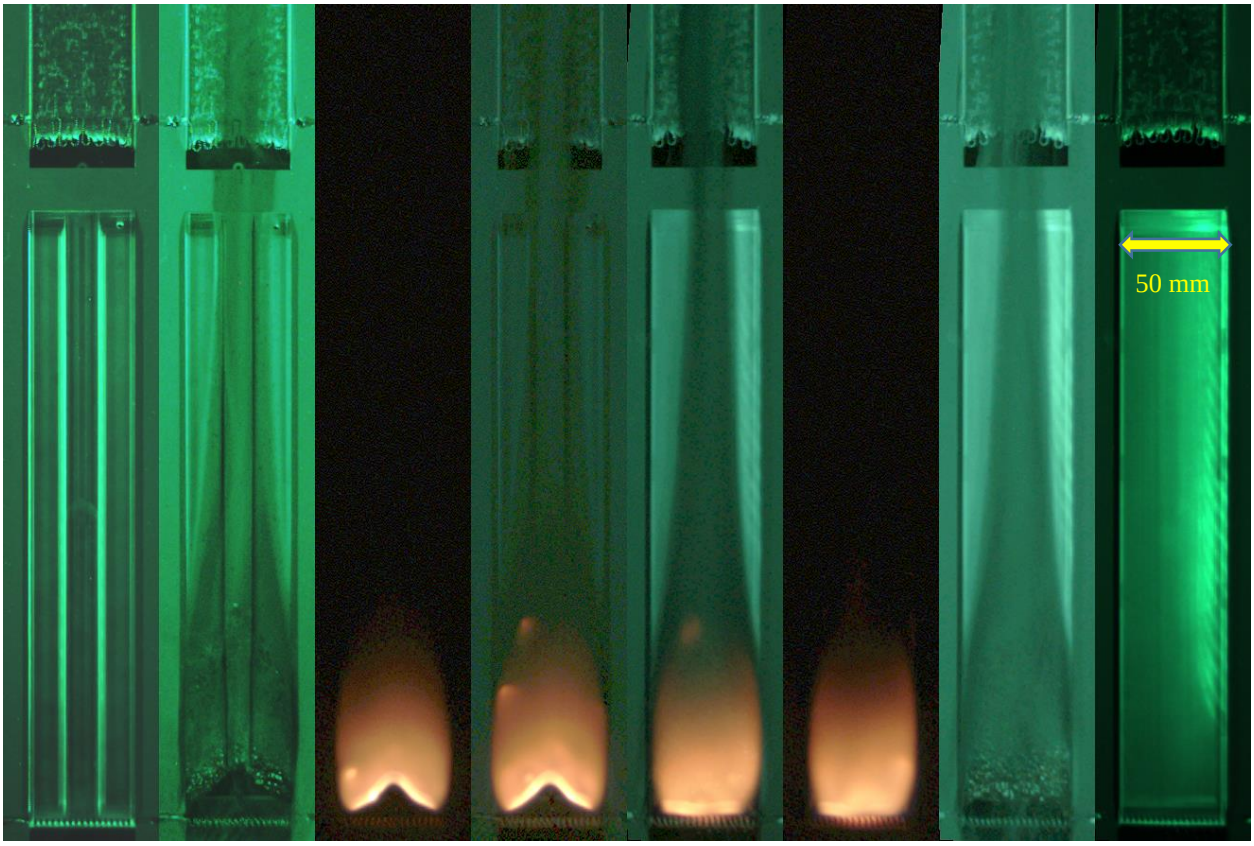

Figure 5: Flame images from the grooved sample 8 (leftmost 4) and the flat sample 9 (rightmost 4). Outside to inside are lit pre- and post-burn, and unlit late burn and lit late burn, respectively.

To show the flame growth with time in each case, the dark frame stills shown in Fig. 6 were averaged over 50 frames to smooth out the vapor jetting. The vapor jetting from MMA vapor bubble ruptures at the surface caused frequent flame shape distortions that grew worse as the test progressed, so averaging frames allows for a clearer picture of the overall flame growth without distortion. The time between images is not the same (because of the sometimes irregular downlinked image frame rate), but the 50 frame averaging occurs over very approximately 6 s for the grooved sample 8 and 11.8 s for the flat sample 9. The first frames average the ignition process, and the flame shrinks significantly in each case after the igniter is turned off. The average for the last few frames include the flame extinction after the flow was turned off. The camera exposure times did not allow for imaging of any blue in the flame base, but it is likely that there is a blue outer flame base that is not visible but is still heating the igniter wire to glowing, and is thus not accounted for in the flame size measurements presented here.

Shortly after the igniter was turned off, the flame for the grooved sample 8 (top part of Fig. 6) initially had a shape that reflected the grooves in the sample. The exposed flame edges had propagated further than the flame body, giving a blue flame wing-like appearance. The central section of the flame over the thinner cross section region also had a longer flame.

While the center section continued to grow, the left 'wing' (1.25 mm radius exposed edge) shrank, and the right wing (sharp edge) was subsumed into the growing center section. This is remarkable because, in normal gravity, the sharper the exposed edge radius of curvature, the faster the flame propagation [26]. The reason is assumed to be two-fold: on the one hand, the burning outer edges are only 4 mm above, the sample holder, and heat loss to the holder can quench the edges of the flame. This quenching effect was clearly shown in 1g tests with different (closer) distances of the edge from the holder card [26] and the effect is expected to be stronger in microgravity. On the other hand, the center section of the flame has enhanced radiation heat transfer within the groove, a larger surface area, and a thinner fuel to

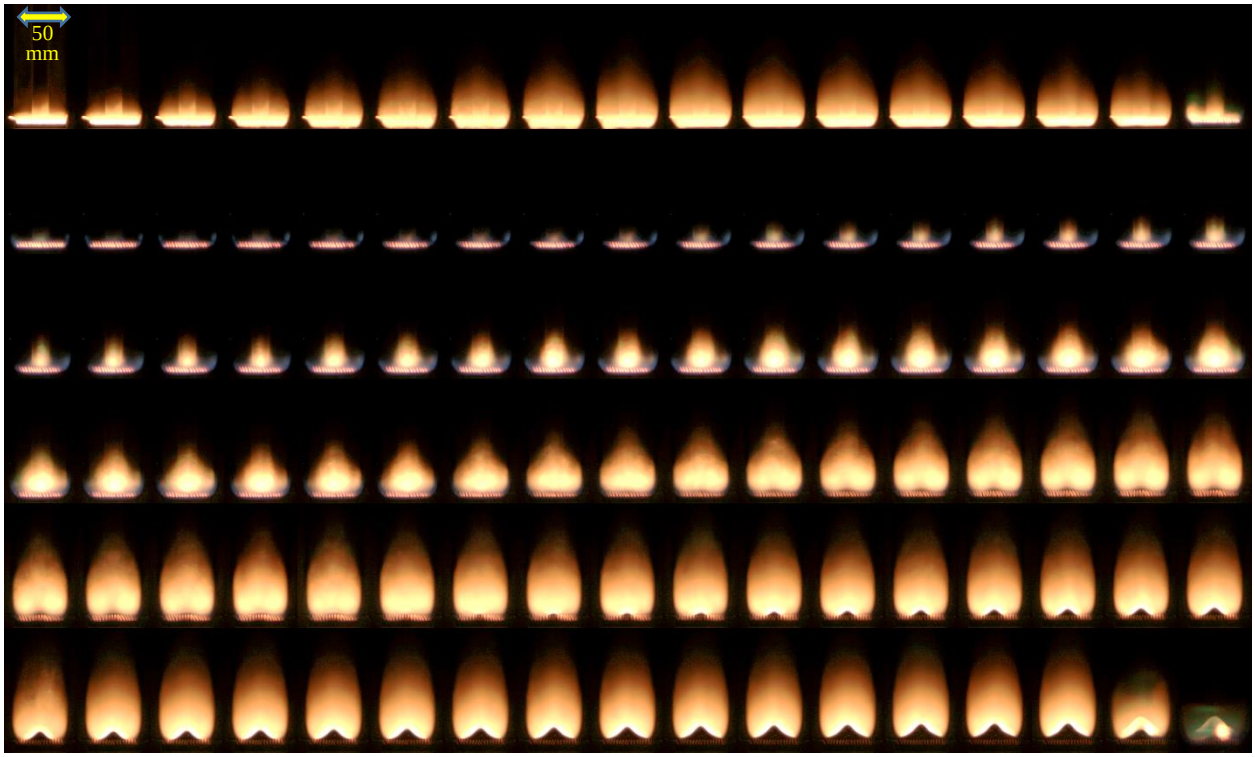

Figure 6: A sequence of images from the grooved sample 8 (above), and from the flat sample 9 (below). The images are 50 frame averages to smooth out the perturbations caused by vapor jetting. All images have the same scale.

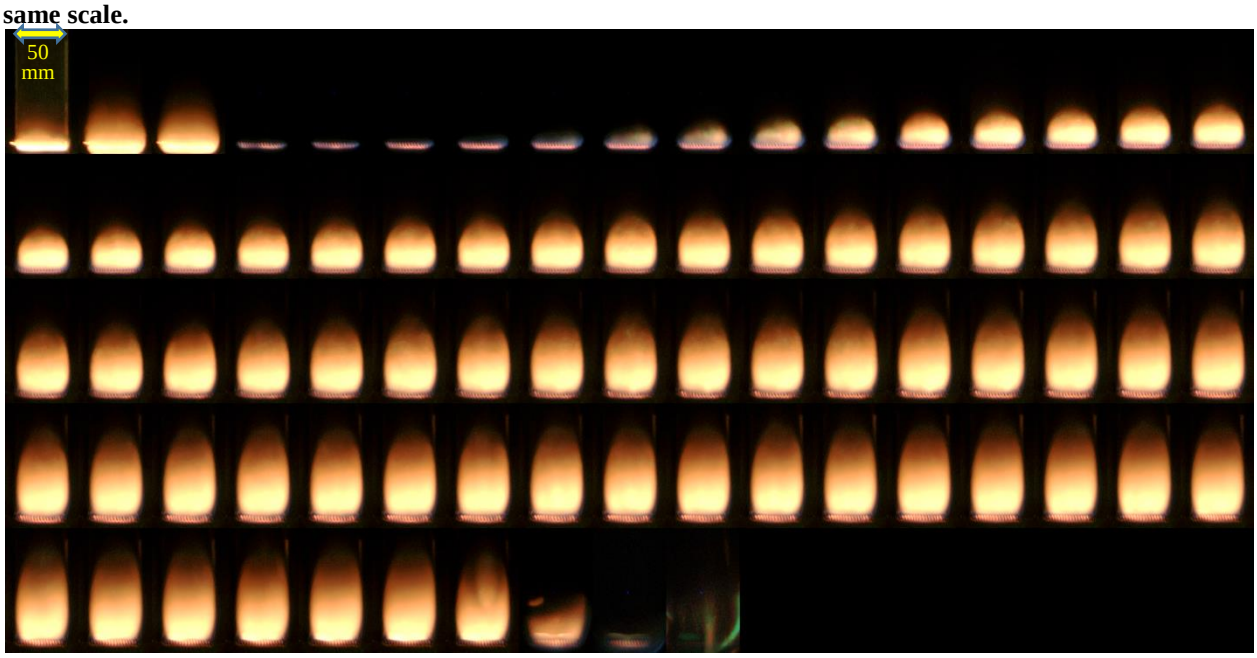

preheat. The tip of the flame is rounded while the base develops a deep notch as the thin center section burns away. The bright sooty base of the flame also has an inverted V shape.

The post-ignition flame for the flat sample 9 was very small and flat, and grew with a flat base and a curved tip. Late in the experiment, the bright, sooty base of the flame is mostly uniform across the width of the sample, and the tip appeared to maintain its parabolic shape. Note that the igniter coil was glowing even late in the test due to heating from the flame.

3.2 Flame Development and Regression Rate

Figure 7 shows the flame tip and base positions as a function of time as obtained from the averaged images from Fig. 6. The tracking started after the igniter was turned off. The base positions of the grooved sample 8 were tracked along both 10 mm thickness side sections and along the centerline. All position data was zeroed at the initial flame base position, which is the standoff distance below the edge of the sample base. The base position of the flat sample 9 was just tracked along the centerline. The tip positions were taken along the centerline for both samples. The flame lengths were simply the difference between the tip positions and the relevant base positions. Note the last few frames where the flame is extinguishing as part of the 50 frame average were also not used.

After ignition, the flame tip for the grooved sample 8 spreads quickly across the sample, and then plateaus out after about 250 s. The flame tip of the grooved sample grows and reaches a steady position much faster than that of the flat sample 9, which did not plateau until 650 s., but both tips eventually extend 90-100 mm downstream.

The flame base for the grooved sample 8 starts to regress at 250 s, with the thin center section regressing more quickly than the thicker side sections. The calculated flame lengths (flame tip-flame base) for each section are included in Fig. 7. The left and right flame lengths appear to be nearly steady at about 80 mm ± 2 mm. Linear regression fits through the flame base data after 300 s are shown. The apparent local spread rates do not correlate with the local thickness. The centerline length appears to shrink considerably due to the faster regression (burnout) of the centerline. One can reason that the overall flame length is controlled by the flame bases of the anchored on the upstream thicker sections. Given the three-dimensional nature of the grooved sample, one must consider the effect of the notch in the flame base to ascertain if the overall flame of the grooved sample will reach a stable shape, as discussed later.

For the flat sample 9, which had a 50% longer experimental run time, it is surprising that the flame base shown in Fig. 7 was just beginning to regress by the end of the experiment, and only spread a handful of pixels before the end of the test (stair step position versus time on right axis of right plot in Fig. 7). The flame regression did seem to be accelerating, given the higher R^2 value of the polynomial fit. The flame length initially grew significantly more slowly than the grooved sample, and the tip position did not catch up to the tip position of the grooved sample until about 550 s. The flame length appears to have reached a steady state of approximately 95 mm ± 2 mm after about 650 s. The

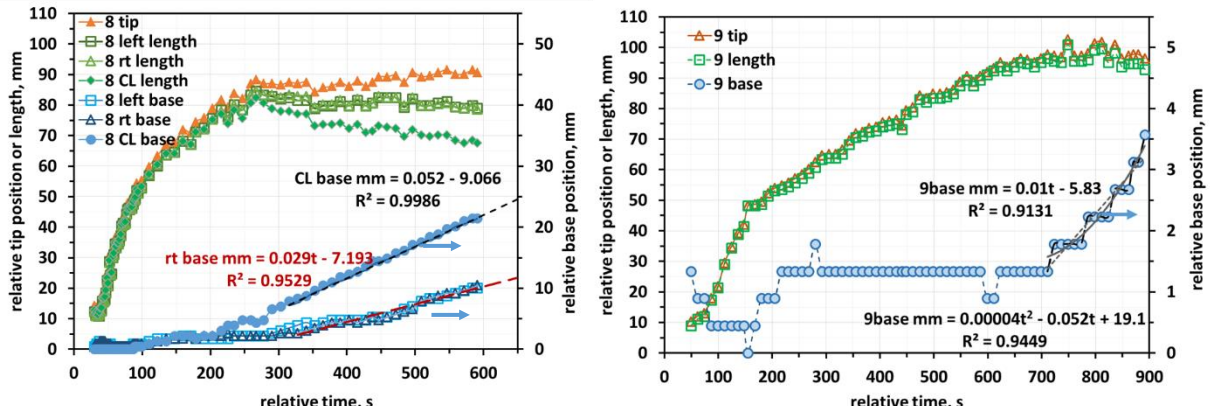

Figure 7: Flame tracking of 50-frame averaged images from Fig. 6. Left: Grooved sample 8; Right: Flat sample 9.

experiment duration of the flat sample was not long enough to determine if the base regression would be similar to the regression rate for the thicker section of the grooved sample.

The data for both tests shows that the flame reached a 'limiting length' [22] for at least 250 s (grooved sample: 350-600 s; flat sample: 650-900 s). The limiting length has been shown to be caused by a zero net heat flux at the flame tip, when flame convective heat flux is offset by surface radiative loss [22]. Note however, that this steady length is achieved by 10 min, not after 100 min as in the previous study [22], possibly due to the difference between an ideal infinitely thick sample and a finite 10 mm thick real sample as well as the difference in convective heating at the modelled 50 mm/s and the experimental 200 mm/s.

While the Saffire PMMA experiments appear to reach a steady size, similar experiments in normal gravity did not reach a steady flame size [25-27]. The upward normal gravity flames were much larger and grew much faster. However, the 1g flat and grooved side base burnout (regression) rates were similar to the Saffire grooved sample, as shown in Table 1. The flat sample's regression had only just begun at the end of the test, but it was accelerating, so the final, steady value, if any, is unknown.

Note that the centerline regression for the grooved sample is slower for the experiments in Saffire II than in 1g [25, 26], possibly due to the oxygen shadow effect from the upstream flame [29], where oxygen is consumed and does not penetrate beyond a certain point within the notch. The centerline regression rate from the microgravity experiments may eventually match the side regression rates due to this oxygen shadow effect, as discussed further in the following.

In microgravity the oxidizer and fuel profiles across the diffusion flame remain stratified due to the lack of vorticity-induced air entrainment. The upstream part of the flame consumes the oxygen and downstream fuel vapor exits beneath the flame tips without reacting. The exception to this is local vapor jetting, where the MMA vapor bubbles rupture at the surface of the molten material and eject the fuel vapor through the flame sheet to the oxidizer outside the sheet, where it subsequently burns. The unburned fuel vapor escaping from the open downstream end of the flame can build up to reach the lean flammability limit for long-burning flames in small spaces. If an ignition source ignites this mixture, it can cause a backdraft, resulting in significant damage or even rupture of the vehicle.

Table 1: Flame base regression rates, mm/s

Sample, location	1g [25]	Saffire II
Grooved , centerline	0.08	0.05
Grooved , sides	0.03	0.03
Flat , centerline	0.03	0.01 (accelerating)

Unlike in upward flame spread in normal gravity (and also likely in upward flame spread in partial gravity) where buoyant flow promotes acceleratory flame growth, the flame reaches a steady size in microgravity with a fixed forced convective flow. This is a significant finding for spacecraft fire safety because it implies that the base regression rate of the material will control the spread rate of the flame for flames anchored at the fuel base. If the flame is limited in length due to balance of convective heat flux to radiative loss from the surface, then the flame size will be limited by the ventilation system's convective velocities in the spacecraft, which are historically fairly low. Because flame sizes are likely to be fairly small, this also makes flashover unlikely in a spacecraft since a small flame is unlikely to produce enough radiation to heat sufficient materials to their ignition temperature. However, ignition of materials in close proximity to a burning material have ignited [10]. Both Saffire II PMMA samples extinguished quickly once the flow was turned off, which supports the existing fire mitigation strategy on the ISS to deactivate the ventilation system in the event of fire alarm.

The solid phase response time is estimated to be $\tau \sim \ell^2/\alpha \sim 200$ s for PMMA with solid phase thermal diffusivity of α=0.12 mm^2/s and ℓ= 5 mm for the half-thickness of the thickest part of the samples. Thus, the flame base did not begin to regress significantly until after the solid phase thermal profile was established. Note that if the full thickness were to be used, the solid phase response time would be 800 s. The actual regression response appears to fall somewhat between these two times, where the grooved sample was closer to the former, and the flat sample was closer to the

latter. For the flat sample, the flame had barely cleared the igniter region by the end of the experiment, so the igniter end could still be influencing both the flame growth and the burnout. For the grooved sample, it may be that the non-uniform notch-shaped burnout had not reached steady state. However, it is likely that the same limiting length principles mentioned above will hold, and a steady-state length and flame shape would result.

Sample geometry clearly played an important role in the flame growth and steady shape. Unlike the normal gravity tests, the exposed edges of the sample did not appear to significantly impact the flame growth. However, the thickness variation had a major impact on the flame growth. The grooved sample developed a deep inverted-V shaped notch as the thin center section burned through, which enhanced flame to solid phase heat transfer through an effectively wider flame base, which is the part of the flame with the highest temperature. Accordingly, the flame over the grooved sample achieved a steady size (limiting length) faster, and the radiation from this stronger flame was significantly higher, as evidenced by the camera exposure times mentioned in Section 3.0 and as will be shown in the radiometer data in Section 4.1.

The angle of the notch (i.e. 2β) was tracked in Fig. 8 from the image sequences shown in Fig. 6 as it became clearly visible in the images. The notch was initially slightly less than 150 degrees ± 5 degrees but narrowed and appears to plateau at approximately 96 ± 5 degrees for the last 100 s of the experiment. This trend is compared with the estimated trend from the linear regression fits of the flame bases by plotting 2β = 2*arctan(16 mm/(CL base mm-right base mm)). As shown in the flame inset to Fig. 8, the opposite side length to angle β is not the full half-width of the sample, but is estimated to be only 16 mm. The adjacent side length is the difference between the centerline position and the right base position, which are estimated from the linear regression fits as functions of time. The 2β estimate does not plateau, but continues to decrease well below the observed angle when extrapolated in time. It is hypothesized that the notch depth will be limited by the oxygen shadow [29] cast by the upstream flame sections, and thus the notch angle should reach a steady state as the flame base spread rate (regression rate) reaches steady state.

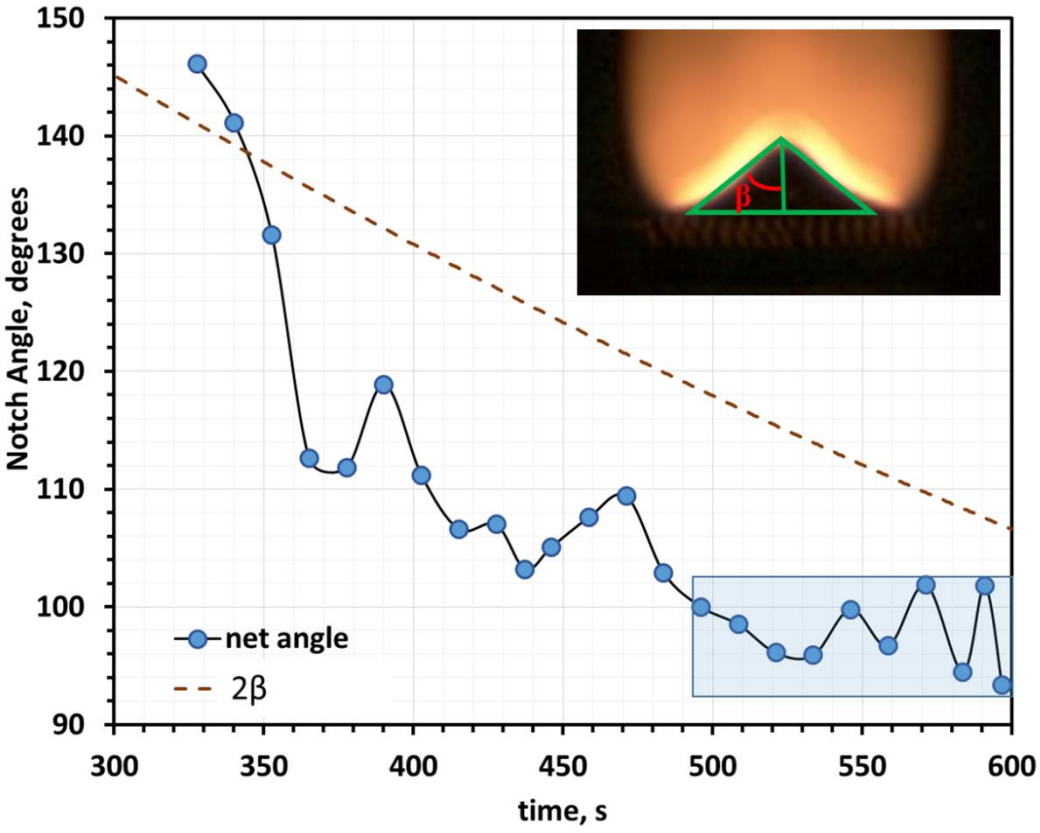

Figure 8: Angle of the notch in the base of the flame for the grooved sample 8 as a function of time, compared with a geometric estimate based on the linear base regressions.

4. Digital sensor readings

A number of other sensors provide comparisons between the two microgravity experiments. The upstream radiometer readings, the thermocouples on the downstream sample, the CO_2 sensor, pressure sensor and the vehicle smoke detector are reported here. The CO_2 sensor was located approximately 80 mm from the inlet of the flow duct in the Saffire cooling flow system to obtain a well-mixed reading.

4.1 Radiometer readings

The two upstream radiometers indicated in Figs. 1 and 2 provided a reading of the flame emissions from each side of the samples. The view factor is not identical for the two samples, so to attempt to correct for this difference, the igniter intensity was normalized for each reading based on the assumption that it was the same for each test. As shown in Fig. 9, the radiometer readings for the grooved sample 8 are significantly higher than the ignition reading, and there is a significant discrepancy between the two readings, indicating that the flame on the back side of the sample (not visible from the camera view) was significantly stronger than the front flame. This is consistent with a higher flow rate noted on the back side of the sample, as shown in Fig. 4. It seems likely that the flame caused the flow imbalance on the two sides of the sample, since the flow started out uniform on both sides and was uniform for the other samples on this flight. This flow imbalance persisted into the early part of the experiment with the flat sample 9.

The flame was significantly weaker throughout the duration of the flat sample experiment, even weaker than the normalizing igniter glow. The flame took significantly longer to rise above the radiometer background reading. The back side flame took even longer to grow despite the fact (or because of the fact) that the backside flow was higher through approximately 400 s of the test. After the flow rebalanced, the back side flame increased in intensity, and the two radiometer readings became evenly matched for the remainder of the experiment.

Notice that the radiometric output continued to increase for the entire duration of the experiment, indicating that the overall flame strength was increasing. The flame moves very little (see the tip position of the grooved in Fig. 7) from 300-600 s, so the increase in radiometer signal is not due to flame movement. It is possible that the gas-phase flame had reached a pseudo-steady-state length while the solid phase thermal profile continued to develop downstream of the flame zone, reducing the heat loss from the flame as the fuel (and surrounding holder) became more preheated. Vapor jetting became stronger as the test progressed as well, further indicating the solid phase preheating and in-depth pyrolysis were strengthening the flame luminosity. Notice that the radiometer reading immediately drops to background levels when the flame extinguishes, indicating that the hot fuel surface and surrounding heated holder are not significantly contributing to the radiometer signal.

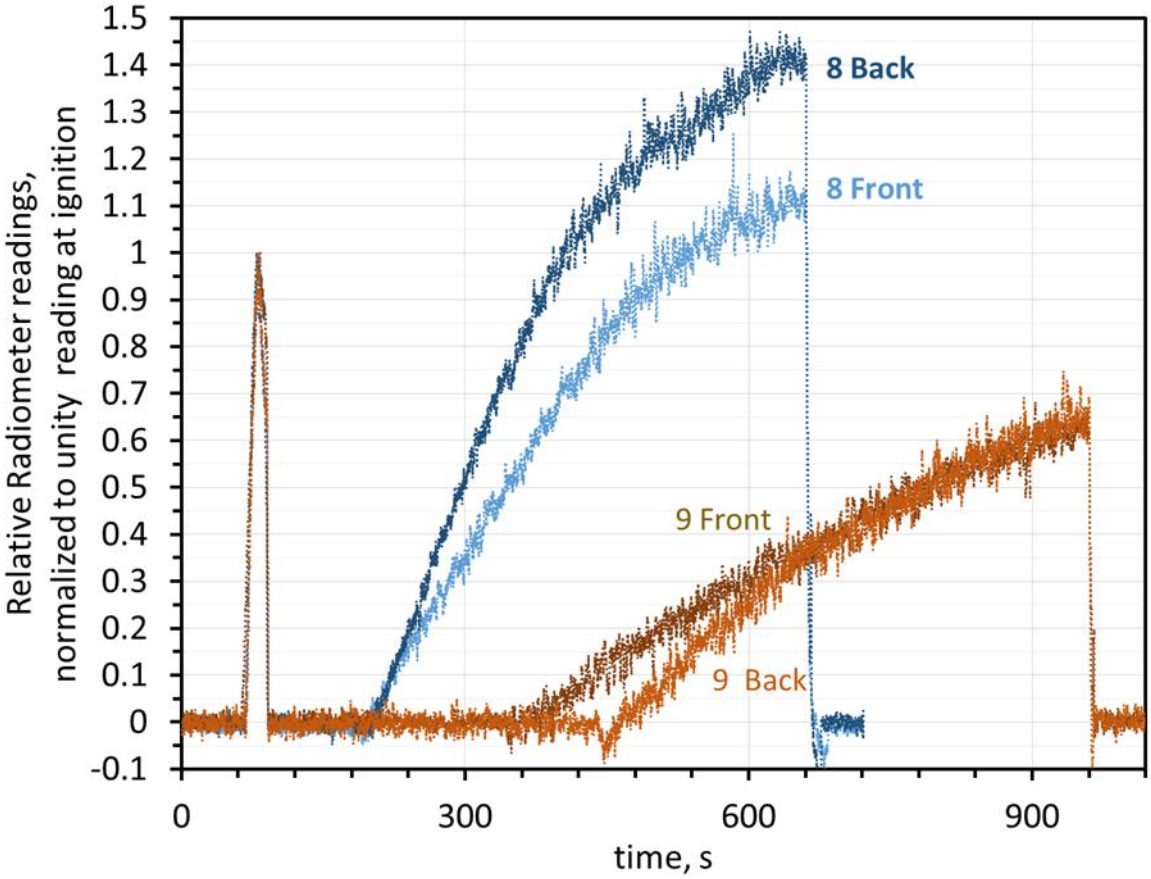

Figure 9: Radiometer reading from both sides of each sample, normalized by the igniter intensity.

It is proposed that the grooved sample's higher radiometer reading is partly due to an effectively wider sample base due to the notch. The flame base, which is the most luminous part of the flame, is approximately 50 mm wide for the flat sample, but the grooved sample has an effective base width of 61 mm due to the notch (22% wider). The higher signal may also be partly due to the increased preheating of the solid from the increased area for conductive preheating caused by the effectively wider base which, as above, will decrease the heat losses to the solid and strengthen the flame.

4.5 Downstream thermocouple readings

Although there were no thermocouples on the PMMA samples, there were surface thermocouples on the SIBAL cloth (samples 5 and 6) [15] just downstream of each PMMA sample. These type R thermocouples (standard accuracy ± 1.5 °C) were 395 mm downstream of the ignition end of grooved and flat samples, along the centerline of the samples, but they still picked up the thermal plume from the PMMA tests, as shown in Fig. 10. It is clear from the thermocouple traces that the grooved sample had a more vigorous ignition and rapid flame development. It also had a stronger plume with a higher downstream temperature. This is consistent with the radiometer data and the camera imaging of a brighter flame. The fact that the downstream temperature appears to reach a plateau for the grooved sample indicates that the surface of the thin SIBAL fuel is in equilibrium. The convective heat flux from the plume is offset by the radiant heat loss from the surface (consistent with the limiting length theory [22]). Assuming the thin fabric is thermally thin and with ε=0.8, the downstream heat flux becomes

$\dot{q}'' = \varepsilon\sigma(T_s^4 - T_\infty^4)$ = 0.0197 W/cm^2 (grooved sample);
= 0.0175 W/cm^2 (flat sample).

These estimates indicate that the grooved sample had slightly more downstream heat flux than the flat sample (13% more) under the same nominal test conditions, which is consistent with the higher radiometer readings and brighter flame images for the grooved sample. Another possible explanation for the higher readings downstream of the grooved sample is that since this sample had a centerline groove that was significantly thinner (4 mm) than the flat sample (10 mm), the thermal boundary layer might have been channeled closer to the centerline surface thermocouple downstream of that groove.

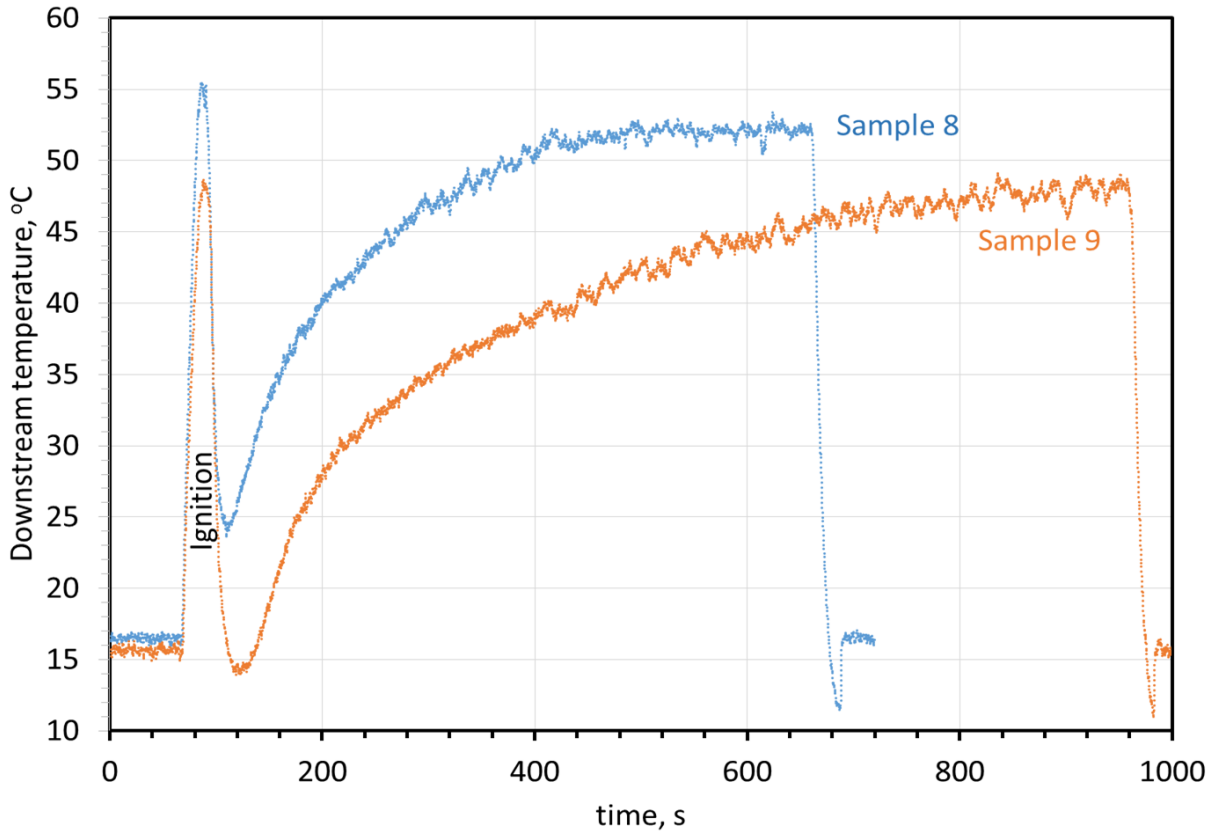

Figure 10: Downstream surface thermocouple readings heated by the thermal plumes from the PMMA samples.

4.5 Pressure Rise

The Cygnus vehicle had a pressure transducer that picked up the overall vehicle pressure rise during each test, as shown in Fig. 11 (left). The pressure sensor was intended to record vehicle atmospheric pressures, not the very small pressure rises recorded here, and the signals are therefore quite noisy, but with a clear trend. The vehicle was in no danger of over-pressurization from these small flames. Once again, the grooved sample had a more rapid and higher pressure rise due to the overall rise in the vehicle air temperature from the combustion event. Notice how once the flow was turned off and the flame extinguished, the pressure began to fall as the vehicle ventilation continued to distribute the heat from the combustion event throughout the large thermal mass of the vehicle.

4.4 Carbon Dioxide

The carbon dioxide sensor also picked up an increase in the ambient level of CO_2 for each combustion test. The increase in CO_2 for each test is shown in Fig. 11 (right). Consistent with a stronger flame for the grooved sample, 50% more CO_2 was produced by the end of 600 s than for the flat sample at the same time. The total CO_2 generated was higher for the flat sample than for the grooved sample due to the longer burn time, but not the 50% more that one would expect for the 50% longer burn time. It therefore seems clear that the grooved sample had a higher burning rate.

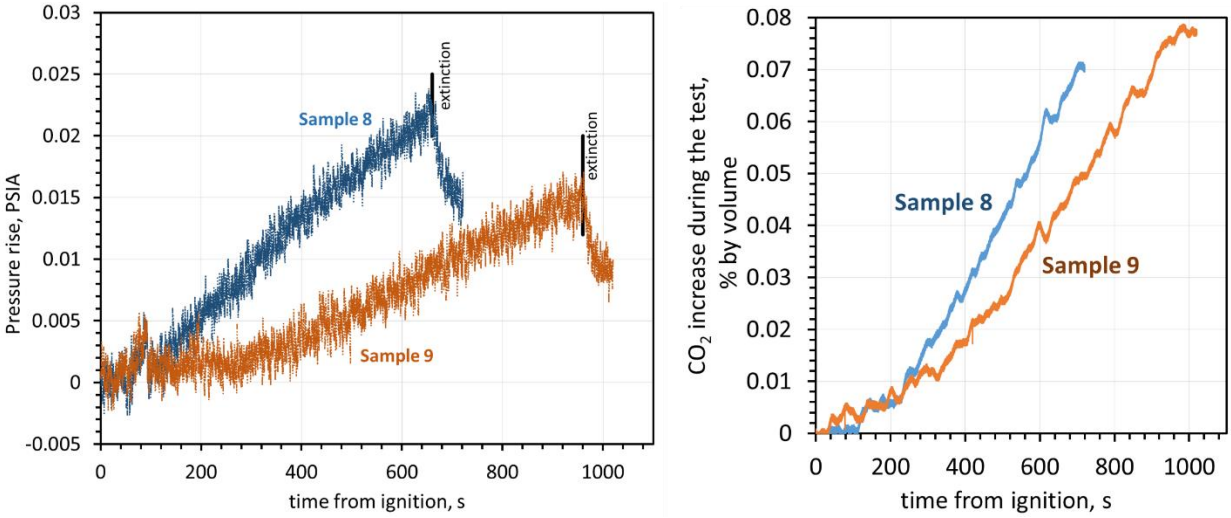

Figure 11: Pressure rise (left) and CO_2 increase in the vehicle as a function of time during each test.

Part of the increase in pressure may be due to the generation of additional moles of gas. The stoichiometry for complete PMMA combustion is

$$C_5H_8O_2 + 6O_2 \rightarrow 5CO_2 + 4H_2O$$

As one can see, for every six oxygen molecules that are consumed, nine molecules of combustion products are produced (assuming the ambient nitrogen is inert). As the vehicle does not reach 100% relative humidity during the testing (whereupon the water vapor would begin to condense), the vehicle pressure will increase due to the increase in moles of gas.

Figure 12 shows the pressure rise as a function of the CO_2 increase. It is interesting to note that the flat sample had less pressure rise for a given generation of CO_2. This is likely due to a lower burning rate that allowed more heat dissipation and thus less pressure rise. Based on the total CO_2 rise divided by the burn time, the burning rate of the grooved sample was 33% higher than for the flat sample. Also notice that even after the flame extinguishes (pressure drops), the CO_2 concentration continues to increase slightly. This is likely due to better mixing of the combustion gases at the sensor. Since the free volume of the vehicle is not known (it is filled with an unknown volume of garbage by the ISS crew before undocking), it is not possible to quantitatively calculate heat release rates or burning rates based on these data.

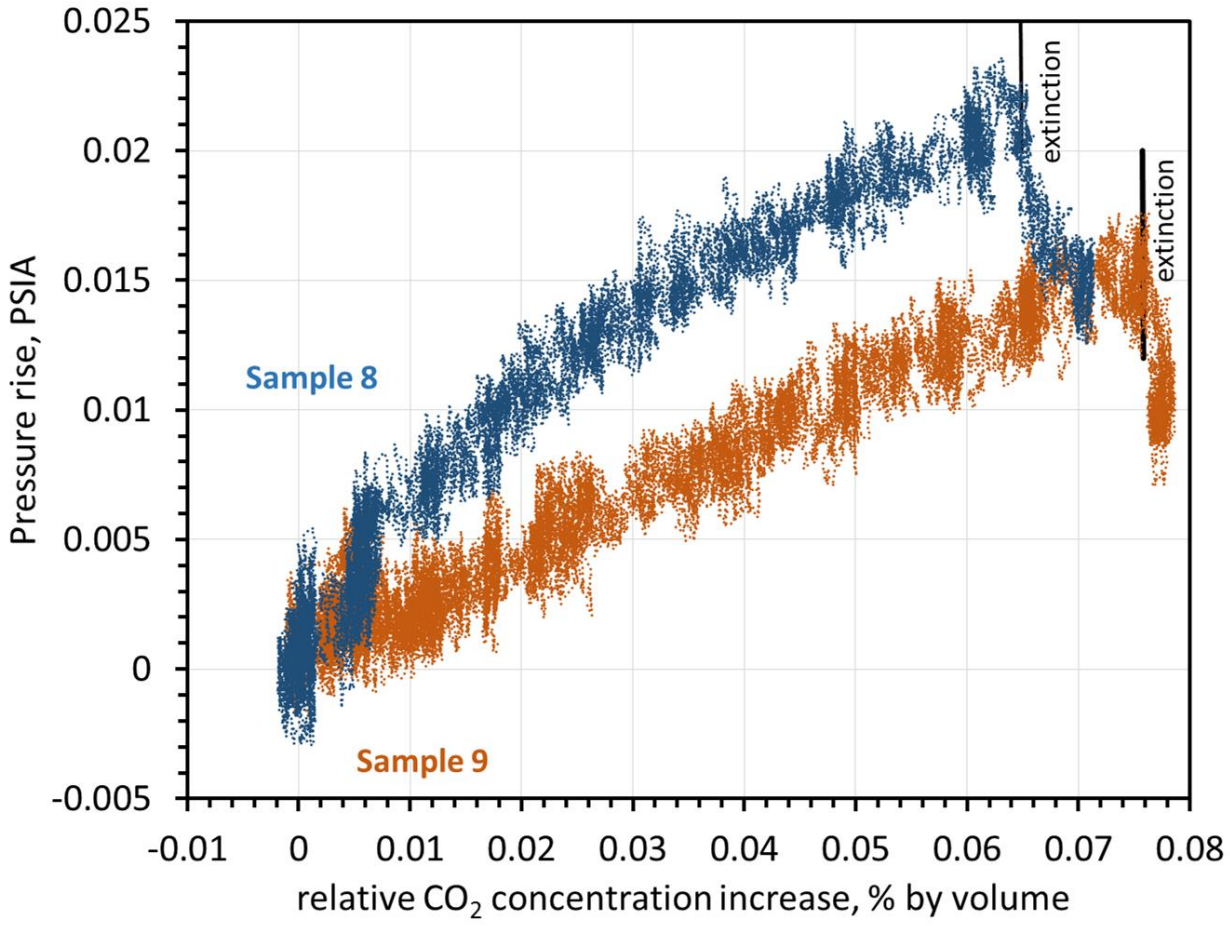

Figure 12: Pressure rise as a function of the CO_2 generated during the experiments.

4.5 Cygnus' Smoke Detectors

The Cygnus vehicle used for the Saffire II tests had a smoke detector that provided a direct obscuration reading of an IR laser beam, and a second forward scattered light reading of that same laser beam. The normal response to a smoke alarm aboard the ISS is to deactivate the ventilation as a fire suppression action. However, this response was intentionally deactivated in the Cygnus vehicle, and the vehicle ventilation continued to operate despite the smoke alarm. It should again be noted that the nominal fire suppression action of deactivating the flow worked in the large volume of the Saffire duct – flames went out when the flow was turned off.

The forward scatter part of the detector picked up the smoke signals from both the grooved and the flat sample, as shown in Fig. 13. The nominal background voltage for the scatterometer was 0.05V. Similar to the previous readings, the grooved sample had a higher smoke detector reading than the flat sample. Interestingly, the ignition event triggered the highest readings during the flaming portion of the test, but in the interim between tests, when the flow restarted in the duct in preparation for the ignition of the flat sample, the residual smoke flushed out of the duct had the highest reading of all. Soot agglomeration may have occurred in the duct, increasing the soot particle size and thus increasing the scattering. Alternatively, or in addition, the still hot PMMA would have continued to pyrolyze for a time, creating an elevated concentration of MMA vapor that may have condensed into a cloud of fuel droplets that would have been measurable by the smoke detector.

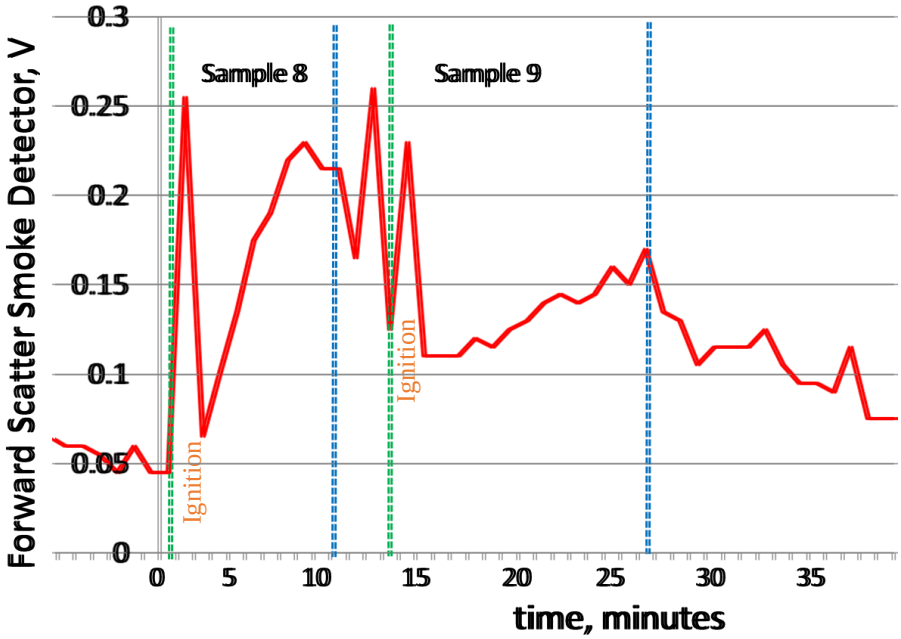

Figure 13: The smoke detector readings from part of the experimental sequence, which included each ignition and subsequent flame growth. Notice that smoke persists after the end of the experiment with the flat sample. A spike in the smoke is seen when the flow turns back on at the start of the experiment with the flat sample as the residual smoke from grooved sample experiment is flushed out of the duct.

5. Conclusions

One grooved and one flat thermally thick PMMA sample were burned in microgravity at 100.6 kPa in an air flow of 200 mm/s. Unlike in normal gravity (and also likely in partial gravity) where buoyant flow promotes acceleratory upward flame growth, the microgravity flames reached a steady size (limiting length) for a fixed forced convective flow in agreement with theory where there is a zero net heat flux at the flame tip. The limiting length implies that the spread rate of the flame will be controlled by the regression rate (burnout rate) of the material since the flames remained anchored to the upstream end of the fuel samples. This is a significant finding for spacecraft fire safety, and makes the probability of flashover in a spacecraft unlikely since flame size will be small for low convective ventilation flow environments typical in spacecraft. On the other hand, long-burning flames in small vehicles will generate significant quantities of fuel vapor that may reach the lean flammability limit and cause a backdraft. The rapid extinction of the flame when the flow was turned off also supports the existing fire mitigation strategy on the ISS to deactivate the ventilation system in the event of fire alarm.

The sample geometry clearly played an important role in the flame growth and steady-state flame shape. Unlike the normal gravity tests, the exposed edges of the sample did not appear to significantly impact the flame growth in the microgravity experiments. However, the thickness variation had a major impact on the flame growth. The grooved sample developed a deep inverted-V shaped notch as the thin center section burned through, which enhanced flame to solid phase heat transfer through an effectively wider flame base, which is the part of the flame with the highest temperature. Accordingly, the flame over the grooved sample more quickly achieved a steady size (limiting length), and the radiation from this stronger flame was significantly higher.

The flame affected the vehicle by raising the ambient pressure slightly, increasing the ambient CO_2 levels (and presumably the humidity), and contaminating the atmosphere with soot particulates that were detected by the smoke detector. The flame locally affected the flow through the Saffire flow duct, creating an imbalance in the flow on the two sides of the sample for the grooved sample.

Acknowledgments

The support of the NASA Advanced Exploration Systems Division provided the finances that enabled the Spacecraft Fire Safety Demonstration Project and the Saffire experiments. The authors appreciate the support of Orbital ATK for the integration and operation of the Saffire experiment in the Cygnus vehicle. The support from the topical team (ESTEC contract number 4000103397) on fire safety in space is also appreciated. In addition, the authors acknowledge the various space and research agencies that have supported the topical team, including but not limited to JAXA, ESA, RSA, CNES, DLR, the Russian Academy of Sciences and NASA.

References

[1] Pedley, M. D., JSC 29353B, 'Flammability Configuration Analysis for Spacecraft Applications', July, 2014.

[2] ECSS, 5. February 2010, "ECSS-Q-ST-70-21-C", ESA Requirements and Standards Division, 2010.

[3] ISO, "ISO 14624-1A Space systems — Safety and compatibility of materials — Part 1: Determination of upward flammability of materials", 2008.

[4] "NASA-STD-6001B, Flammability, Offgassing and Compatibility Requirements and Test Procedures", NASA, 2016.

[5] Jomaas, G., Torero, J.L., Eigenbrod, C., Niehaus, J., Olson, S.L., Ferkul, P.V., Legros, G., Fernandez-Pello, A.C., Cowlard, A.J., Rouvreau, S. and Smirnov, N., "Fire safety in space–beyond flammability testing of small samples", Acta Astronautica, 109, 2015, pp.208-216.

[6] Altenkirch, R. A., Tang, L., Sacksteder, K., Bhattacharjee, S. and Delichatsios, M. A. "Inherently unsteady flame spread to extinction over thick fuels in microgravity." *Proc. Combust. Inst.* Vol. 27, no. 2, 1998, pp. 2515-2524.

[7] Ferkul, P., Sacksteder, K. Greenberg, P., Dietrich, D., Ross, H., Tien, J., Altenkirch, R. Tang, L., Bundy, M. and Delichatsios, M., "Combustion experiments on the Mir space station." *37th Aerospace Sciences Meeting and Exhibit*, 1999, p. 439. AIAA-99-0439.

[8] Sanchez-Tarifa, C., and Lazaro, B., "Experiments Conducted on Combustion of a Solid at Microgravity in the Texus-38 Sounding Rocket. Results and Conclusions". *Microgravity Research and Applications in Physical Sciences and Biotechnology* Vol. 454, 2001, p. 267.

[9] Olson, S. L., Hegde, U., Bhattacharjee, S., Deering, J. L., Tang, L., and Altenkirch, R. A., "Sounding rocket microgravity experiments elucidating diffusive and radiative transport effects on flame spread over thermally thick solids." *Combustion science and technology* 176, no. 4, 2004, pp. 557-584.

[10] Ivanov, A.V., Balashov, Ye.V., Andreeva, T.V., and Melikhov, A.S., 'Experimental Verification of Material Flammability in Space', NASA/CR—1999-209405, 1999.

[11] Olson, S. L., and Ferkul, P. V., "Microgravity flammability boundary for PMMA rods in axial stagnation flow: Experimental results and energy balance analyses." *Combustion and Flame* 180, 2017, pp. 217-229.

[12] Meyer, F., Schwenteck, T., Ruhe, M., Bihn, P., Freier, A., and Eigenbrod, C., (2017a). Experimental Findings on Flame Propagation along PMMA Samples in Reduced Gravity on REXUS 20 (UB-FIRE). 23rd ESA PAC Symposium. ESA. Visby, ESA. 2017: 8.

[13] Meyer, F., Schwenteck, T., Ruhe, M., Bihn, P., Freier, A., and Eigenbrod, c., (2017b). UB-FIRE Experiment Results on Upward Flame Propagation along Cylindrical PMMA Samples in Reduced Gravity. 47th ICES. Charleston, SC. 2017: 11.

[14] Markstein, G. H., and De Ris., J., "Upward fire spread over textiles." In *Symposium (International) on Combustion*, vol. 14, no. 1, 1973, pp. 1085-1097.

[15] Urban, D. L., Ferkul, P., Olson, S., Ruff, G, A., T'ien, J. S., Liao, Y-T. L., Fernandez-Pello, A. C., Torero, J. L., Legros, G., Eigenbrod, C., Smirnov, N., Fujita, O., Rouvreau, S., Toth, B., Jomaas, G., 'Flame Spread: Effects of Microgravity and Scale', Comb. Flame 199, 2019, pp. 168-182.

[16] Fernandez-Pello, A. C., and Hirano. T., "Controlling mechanisms of flame spread." *Combustion Science and Technology* 32, no. 1-4, 1983, pp. 1-31.
[17] Loh, H-T., and Fernandez-Pello, A. C., "A study of the controlling mechanisms of flow assisted flame spread." In *Symposium (International) on Combustion*, vol. 20, no. 1, 1985, pp. 1575-1582.
[18] Chao, Y. H., and Fernandez-Pello, A. C., "Flame Spread in a Vitiated Concurrent Flow." ASME-PUBLICATIONS-HTD 199 (1993): 135-135.
[19] Delichatsios, M. A., Altenkirch, R. A., Bundy, M. F., Bhattacharjee, S., Tang, L., and Sacksteder, K., "Creeping flame spread along fuel cylinders in forced and natural flows and microgravity." *Proceedings of the Combustion Institute* 28, no. 2, 2000, pp. 2835-2842.
[20] Di Blasi, C., Crescitelli, S., and Russo, G., "Near limit flame spread over thick fuels in a concurrent forced flow." *Combustion and flame* 72, no. 2, 1988, pp. 205-215.
[21] Fernandez-Pello, C., and Mao, C-P., "A unified analysis of concurrent modes of flame spread." Combustion Science and Technology 26, no. 3-4, 1981, pp. 147-155.
[22] Tseng, Y-T., and T'ien, J. S. "Limiting length, steady spread, and non-growing flames in concurrent flow over solids." Journal of heat transfer 132, no. 9, 2010, pp. 091201 1-9.
[23] Raghavan, V., Rangwala, A. S., and Torero, J. L., "Laminar flame propagation on a horizontal fuel surface: Verification of classical Emmons solution." *Combustion Theory and Modelling* 13, no. 1, 2009, pp. 121-141.
[24] Smirnov, E. M., Ivanov, N. G., Telnov, D. S., and Son, C. H., "CFD Modelling of Cabin Air Ventilation in the International Space Station: A Comparison of RANS and LES Data with Test Measurements for the Columbus Module." International Journal of Ventilation 5, no. 2, 2006, pp. 219-227.
[25] Eigenbrod, C., Hauschildt, J., Meyer, F., Urban, D.L., Ruff, G.A., Olson, S.L., Ferkul, P., Jomaas, G. and Toth, B., Experimental results on the effect of surface structures on the flame propagation velocity of PMMA in microgravity. 47th International Conference on Environmental Systems. ICES 2017-67, Charleston, SC, July 2017.
[26] Würzburg, N., "Experiments on the vertical flame propagation along surface-structured PMMA-samples; Influence of sample thickness", Universität Bremen, B.Sc., Universität Bremen, 2015, pp. 1-60.
[27] Thomsen, M., Fernandez-Pello, C., Ruff, G. A., and Urban, D. L., "Buoyancy effects on concurrent flame spread over thick PMMA." Combustion and Flame 199, 2019, pp. 279-291.
[28] Ferkul, P., Olson, S., Urban, D. L., Ruff, G. A., Easton, J., T'ien, J. S., Liao, Y-T. T., Fernandez-Pello, A. C., Torero, J. L., Eigenbrod, C., Legros, G., Smirnov, N., Fujita, O., Rouvreau, S., Toth, B., Jomaas, G. 'Results of Large-Scale Spacecraft Flammability Tests', 47th International Conference on Environmental Systems, Charleston, SC, July 16-20, 2017.
[29] Kashiwagi, T., McGrattan, K. B., Olson, S. L., Fujita, O., Kikuchi, M., and Ito, K., "Effects of slow wind on localized radiative ignition and transition to flame spread in microgravity." In Symposium (International) on Combustion, vol. 26, no. 1, 1996, pp. 1345-1352.